Perforated Wetting Layers from Periodic Patterns of Lyophobic Surface Domains

Peter Lenz,[†,‡] Clemens Bechinger,[§] Claudia Schäfle,[§] Paul Leiderer,[§] and Reinhard Lipowsky*,[†]

Max-Planck-Institut für Kolloid- und Grenzflächenforschung, D-14424 Potsdam, Germany, Lyman Laboratory of Physics, Harvard University, Cambridge, Massachusetts 02138, and Universität Konstanz, Fachbereich Physik, Universitätsstrasse 10, D-78457 Konstanz, Germany

We investigate, both theoretically and experimentally, the wetting morphology of a liquid which is adsorbed onto a chemically structured substrate consisting of circular lyophobic domains in a lyophilic matrix. For thick films, the adsorbate morphology is not affected by the underlying domain pattern but reduction in the film thickness leads to the formation of stable holes and, thus, to perforated wetting films. These perforated films, which exist for an intermediate range of volumes, are bounded by surfaces of both constant mean curvature and high topological genus. By making use of nodoids, we are able to derive an approximate analytical parametrization of these surfaces. This "muffin-tin" parametrization captures the essential features of the wetting layer morphology as shown by comparison with direct numerical minimization of the free energy. Furthermore, the theoretical shapes are in very good agreement with experimental data obtained by atomic force microscopy.

1. Introduction

Minute modifications on surfaces are well-known to influence the wettability of a substrate by an adjacent adsorbate. If, for example, water condenses onto a surface, an irregular pattern of small drops develops (forming so-called breath figures, cf. ref 1) which probes the natural heterogeneity of the surface. In contrast, if the substrate surface is artificially structured, the morphology of the liquid adsorbate is crucially influenced by the underlying pattern of surface domains. The shape of the liquid can then be controlled by adjusting the corresponding geometrical boundary conditions. It has already been demonstrated that the physical properties of these wetting systems depend on their morphology; cf. for example refs 2 and 3. Therefore, these novel possibilities to control the shape might be used in order to produce artificial physical, chemical, or biological systems with unique properties.

Up to now, the theoretical and experimental investigations of such structured substrates have mainly concentrated on their wetting properties.[2−7] These studies are fundamental both for the extension to more complex systems and for possible applications. The theoretical and experimental investigation of the interplay between the geometrical boundary conditions and the morphology of the wetting layer has already led to the discovery of a variety of novel wetting phenomena. Examples are (i) nonspherical droplets which are stabilized by the structure of the substrate.[2,3] Such droplets are unstable on homogeneous substrates against shape deformations which displace their contact line.[5] However, these droplets can exhibit (ii) novel shape instabilities which are characterized by a rearrangement of the liquid within the droplet at fixed contact line.[2,3] Additionally, (iii) morphological wetting transitions between wetting layer morphologies are observed which extend over several domains as for example droplet patterns on an array of circular patches.[4]

In this paper, we extend our studies to a system which has unique topological and geometrical properties. It is given by a wetting layer whose liquid−vapor interface is a constant mean curvature surface of high topological genus. It is stabilized by a lyophilic substrate with many circular lyophobic domains. We derive an analytical description of its morphology and give a detailed mathematical analysis of the geometrical properties of the liquid−vapor interface.

We demonstrate both theoretically and experimentally that the Laplace equation (i.e., the equation which determines the shape of the liquid−vapor interface) indeed has solutions with many "holes", that is, solutions of high topological genus. Furthermore, an exact solution for special geometries is presented (valid for a single hole) and its approximate extension to the many-hole case is compared with numerical solutions. Although these results might appear to be very technical, they are fundamental for any further investigations.

We also show how wetting layers with many holes can be temporarily or permanently stabilized. By use of appropriate sol−gel reactions, the system can be solidified without disturbing its morphology. In this way, the system described here can be seen as a first step toward novel artificial materials which have unique (prescribed) geometrical and topological properties.

We expect the physical properties of this system to be crucially influenced by its morphology. For example, the spectrum of fluctuations will depend on the structure of the substrate: if the domains form a periodic grid on the substrate, the capillary waves will have a band structure. Deviations from the periodicity of the domain array on the substrate might lead to "defectlike" disturbances of

---

[†] Max-Planck-Institut für Kolloid- und Grenzflächenforschung.
[‡] Lyman Laboratory of Physics, Harvard University.
[§] Universität Konstanz, Fachbereich Physik.
(1) Beysens, D.; Knobler, C. M. *Phys. Rev. Lett.* **1986**, *57*, 1433.
(2) Gau, H.; Herminghaus, S.; Lenz, P.; Lipowsky, R. *Science* **1999**, *283*, 46.
(3) Lenz, P.; Fenzl, W.; Lipowsky, R. *Europhys. Lett.* **2001**, *53*, 618.
(4) Lenz, P.; Lipowsky, R. *Phys. Rev. Lett.* **1998**, *80*, 1920.
(5) Lenz, P.; Lipowsky, R. *Eur. Phys. J. E* **2000**, *1*, 249.
(6) Lipowsky, R.; Lenz, P.; Swain, P. S. *Colloids Surf., A* **2000**, *161*, 3.
(7) Lenz, P. *Adv. Mater.* **1999**, *11*, 1531.

the liquid−vapor interface. More generally, it might be possible to use this wetting system as a realization of a soft crystal since many of its physical properties are dominated by symmetry.

Finally, from a mathematical point of view, this investigation is complementary to earlier ones. General arguments suggest[6,8] that the phase diagram derived in ref 4 is valid for a wide class of domain geometries. Thus, one expects that the completely wetting film and the homogeneous and heterogeneous droplet patterns are relevant (and experimentally observable) states in many patterned systems with (topologically) connected lyophobic regions. The system investigated here is topologically different, since the lyophilic regions are connected. Correspondingly, the structure of the substrate is only relevant for a small volume range in which this dewetted state exists. The phase diagram is dominated by the film state.

This paper is organized as follows. First, the theoretical framework for the following study is introduced in section 2. Then, in section 3 the experimental investigation of the liquid structures is described. In section 4, the approximate analytical solution is derived. Next, the results of the numerical minimization are presented and the three approaches are compared. We conclude with a summary and an outlook.

2. Preliminaries

The system which is investigated here consists of an array of N circular lyophobic domains (δ) on a lyophilic substrate (γ). In principle, the arrangement of the domains on the substrate could be arbitrary, but for simplicity we specialize here on a periodic grid. This system is thus complementary to the one studied in ref 4, where a lyophobic substrate with many circular lyophilic domains has been considered. Formally, these two systems can be transformed into each other by interchanging the lyophilic and lyophobic regions. Thus, in the present study, the lyophobic regions of the substrate are spatially separated whereas the lyophilic ones are connected.

Under suitable experimental conditions, which can be realized by for example adding appropriate walls to the system, a completely wetting film exists as a stable configuration. At high volumes, that is, at sufficiently large amounts of adsorbed liquid, the equilibrium configuration of the wetting layer is given by this film which covers the whole substrate. Thus, at high volumes the morphology of the wetting layer is not influenced by the structure of the substrate. However, if the volume is continuously decreased, then for small film heights the structure of the substrate becomes more and more important. Finally, at a critical volume the film state becomes energetically unfavorable since it also covers the lyophobic regions (δ). Then, a morphological wetting transition to a configuration takes place where the lyophobic domains are dewetted. Here, the liquid−vapor interface of the wetting layer is given by a connected two-dimensional surface with many holes. The properties of this dewetted state are investigated in this article by using both experimental and theoretical methods.

In both cases, we will always be interested in the equilibrium configuration of the wetting layer which corresponds to the global minimum of the free energy. To proceed, we denote the vapor and the liquid phase by α and β, respectively; see Figure 1. The interfacial region between phase i and phase j has surface area A_{ij} and interfacial tension Σ_{ij}, with $i, j = \alpha, \beta, \gamma$, or δ. The two
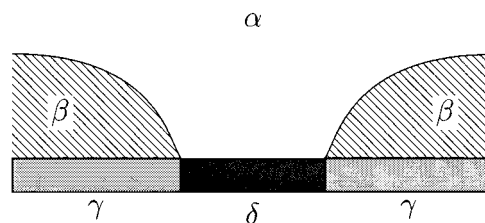

Figure 1. Wetting geometry: a liquid (β) dewets the circular lyophobic domains (δ) on a lyophilic substrate (γ).

surface regions γ and δ are characterized by contact angles θ_γ and θ_δ which are related to the interfacial tensions via the usual Young relations.

The droplet regimes I, II, and III introduced in ref 4 can be distinguished here as well. For small volumes of adsorbed liquid, the wetting layer belongs to regime I. Here, only the γ regions are (partially) covered by spatially separated droplets. In regime II, γ is completely covered, and in regime III also parts of δ are covered. In regimes I and III, the Young equation is fulfilled, whereas in regime II the contact angle is determined by the volume only.

To keep the discussion as simple as possible, we will restrict the analysis to regime II. We will thus implicitly assume that an intermediate amount of volume is adsorbed. Furthermore, we will concentrate on domains and corresponding droplets in the micrometer range. In this situation, the free energy of a wetting layer consists of the contributions arising from the interfacial free energy of the $\alpha\beta$ interface, from the free energy of wetting the contact area and from the volume. Then, if the volume V of the wetting layer is prescribed, its free energy functional is given by[4,6]

$$F(A, V) = \Sigma_{\alpha\beta} A_{\alpha\beta} + A_{\alpha w}(\Sigma_{\beta w} - \Sigma_{\alpha w}) + (P_\alpha - P_\beta)V \quad (1)$$

with $w = \gamma$ or $w = \delta$. The pressure difference appearing in the last term is a Lagrange multiplier which guarantees that the constraint on the volume is fulfilled.

If larger length scales are considered, gravity has to be taken into account (see e.g. refs 9−10), while for smaller scales corrections arising from line tensions (see e.g. refs 6, 11−13) and intermolecular interactions will become important.[14,15]

In the following sections, the wetting layers are studied by experimental, analytical, and numerical methods. In all three cases, we focus on equilibrium configurations corresponding to the global minima of the free energy functional (eq 1).

3. Experimental Investigation

Chemically patterned substrates were fabricated by microcontact printing (μCP)[16] of alkanethiols on gold-coated glass sheets. Since this technique has become well established in the last couple of years,[17] we will only briefly describe our experimental procedure. We printed a 1 mM ethanolic solution of

(8) Lenz, P. Benetzungsphänomene auf strukturierten Substraten. Ph.D. Thesis, University of Potsdam, Potsdam, Germany, 1998.

(9) Finn, R. *Equilibrium capillary surfaces*; Springer-Verlag: New York, 1986.

(10) Brochard−Wyart, F.; Daillant, J. *Can. J. Phys.* **1990**, *68*, 1084.

(11) Widom, B. *J. Phys. Chem.* **1995**, *99*, 2803.

(12) Swain, P. S.; Lipowsky, R. *Langmuir* **1998**, *14*, 6772.

(13) Pompe, T.; Frey, T. A.; Herminghaus, S. *J. Adhes. Sci. Technol.* **1999**, *13*, 1155.

(14) See, for example: Lipowsky, R. *Phys. Rev. Lett.* **1984**, *52*, 1429. Lipowsky, R.; Fisher, M. E. *Phys. Rev. B* **1987**, *36*, 2126.

(15) Koch, W.; Dietrich, S.; Napiorkowski, M. *Phys. Rev. E* **1995**, *51*, 3300.

(16) Kumar, A.; Whitesides, G. M. *Appl. Phys. Lett.* **1993**, *63*, 2002. Kumar, A.; Biebuyck, H. A.; Whitesides, G. M. *Langmuir* **1994**, *10*, 1498.
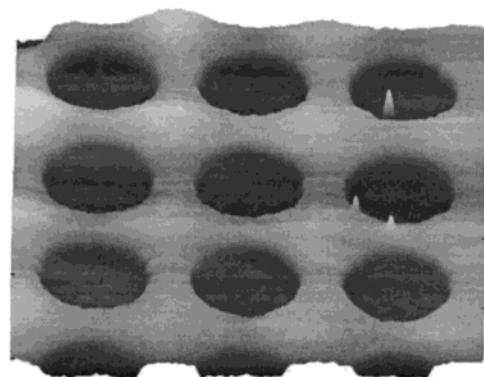
(17) Xia, Y.; Whitesides, G. M. *Angew. Chem., Int. Ed.* **1998**, *37*, 550.

unpolar octadecanethiol $HS(CH_2)_{17}-CH_3$ with a patterned stamp of elastomeric material (poly(dimethylsiloxane)) onto the substrate and subsequently dipped the substrate in a 1 mM ethanolic solution of polar 11-mercaptoundecanol $HS(CH_2)_{11}-OH$. This produces substrates with well-defined arrays of lyophobic and lyophilic domains. The resulting structures were confirmed to have the geometry of the stamp by monitoring the phase signal during imaging of the surface with atomic force microscopy (AFM) in tapping mode.

Liquid structures in the micrometer range can be successfully imaged with AFM in tapping mode.[18] However, this requires the liquid structures under investigation to be stable (e.g., against evaporation) during a typical scan time which is of the order of several minutes. This difficulty becomes even more severe for the system studied here since the dewetted state exists only in a small volume range (see section 5). Therefore, we produced and stabilized such delicate structures by means of a chemical reaction which eventually "froze" the initial liquid into a solid structure and could be imaged by AFM without the aforementioned problems. This solidification is achieved by using highly reactive liquids such as metal alkoxides which are well-known to undergo a gelation process when exposed to air humidity. Since the gelation process starts at the adsorbate surface, this surface shape is stabilized by forming a highly viscous macromolecular network. Therefore, although some volume loss occurs during gelation, the morphology of the adsorbate is essentially preserved in a state where its shape is still dominated by interfacial tensions. As a result, the obtained structures correspond to those of simple liquids.[19]
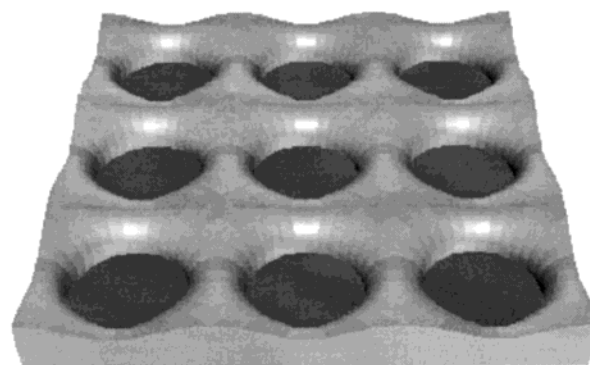
In this process, which is well-known as the sol−gel technique,[20] an inorganic or organic molecular precursor $M(OR)_n$, a sol, is used as the starting material, where M is a metal and (OR) is an organic compound. When such low viscous precursors are applied to substrates by spin- or dip-coating, a macromolecular oxidic network (M−O−M) forms in a moist environment through hydrolysis and polycondensation. This transforms the precursor into a highly viscous (gel-like) hydrated metal oxide MO_x. For details, we refer to the literature.[20] We used two different procedures corresponding to two different precursors: (i) tetraisopropylorthotitanate ($TiC_{12}H_{28}O_4$, TIOT, purchased from Merck Schuchardt) and (ii) tungsten alkoxide. In both cases, it is difficult to measure the values of the contact angles θ_γ and θ_δ directly. However, the comparison between theory and experiment as described in the following clearly indicates that the experimentally observed wetting morphologies belong to droplet regime II with $\theta_\gamma < \theta < \theta_\delta$.

In procedure i, we added ethanol and acetylacetone ($C_5H_8O_2$) with a volume ratio of 1:2:18 in order to improve the dewetting properties of the lyophobic patches. After the sol−gel process is completed, this mixture finally leads to the formation of titanium oxide. Thus, in this system the α phase is air, the wetting liquid β is the TIOT solution, γ is given by OH-terminated thiol, and δ is given by CH_3-terminated thiol SAMs (self-assembled monolayers) on gold substrates. Figure 2a shows a typical result after the TIOT solution has been applied by dip-coating to a substrate composed of lyophobic circular regions which form a square lattice in the lyophilic matrix. The liquid dewetted the lyophobic domains and formed a connected structure. The AFM image was taken after the gelation process of the precursor.

In procedure ii, the tungsten alkoxide precursors were prepared by dissolving 3 g of tungsten hexachloride (WCl_6) in 10 mL of ethanol[21] and adding 10−20 mL of acetylacetone.[22] The final mixture contained also 7 mL of dilute (1 M) hydrochloric acid. Figure 3 shows an example where this precursor was applied to a substrate composed of circular patches (δ) which form a triangular lattice on the matrix (γ). Here, the γ regions are given by CH_3-terminated thiol SAMs and the δ regions are given by OH-terminated thiol SAMs on gold.

(18) Herminghaus, S.; Fery, A.; Reim, D. *Ultramicroscopy* **1997**, *69*, 211.

(19) Bechinger, C.; Muffler, H.; Schäfle, C.; Sundberg, O.; Leiderer, P. *Thin Solid Films* **2000**, *366*, 135.

(20) Brinker, C. J.; Scherer, G. W. *Sol-Gel Science*; Academic Press: San Diego, CA, 1990.

(21) Judenstein, P.; Morineau, R.; Livage, J. *Solid State Ionics* **1992**, *51*, 239.

(22) Guglielmi, M.; Carturan, G. *J. Non-Cryst. Solids* **1988**, *100*, 16.

(a)

(b)

Figure 2. (a) TiO_2 on a substrate with lyophobic circles in a lyophilic matrix as a result from a dewetting process of a liquid sol and a subsequent gelation as obtained via procedure i; see text (size, 9.4 × 9.4 μm^2; height, 35 nm; AFM tapping mode). (b) Wetting layer morphology as determined by numerical minimization as described in section 5. Direct comparison of (a) and (b) shows that the theoretical and experimental morphologies are in fair agreement and exhibit the same characteristics.
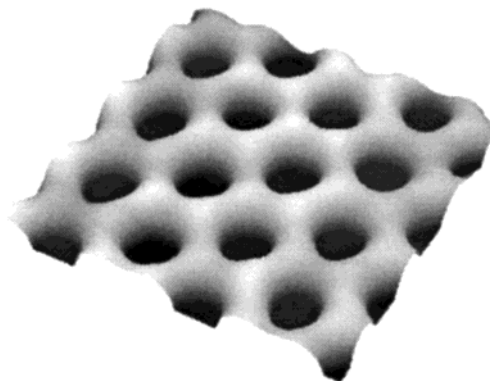

Figure 3. WO_3 structure on a substrate with lyophobic circles in a lyophilic matrix as a result of a phase separation process (lateral size of AFM picture, 11 μm × 11 μm; height, 740 nm). This corresponds to procedure ii as described in the text.

In contrast to case i, the liquid did not dewet the substrate but formed a thin liquid film on the whole substrate which underwent a subsequent microphase separation. During this process, the volatile component preferentially adsorbed at the δ sites thus leaving only the γ areas for the tungsten-containing component. While the volatile component evaporates, the gelation of the tungsten-containing phase is nucleated at the γ regions of the substrate. Correspondingly, the wetting liquid β is here given by the tungsten alcoholate and the α phase corresponds to the volatile component of the solution.

(a)   (b)

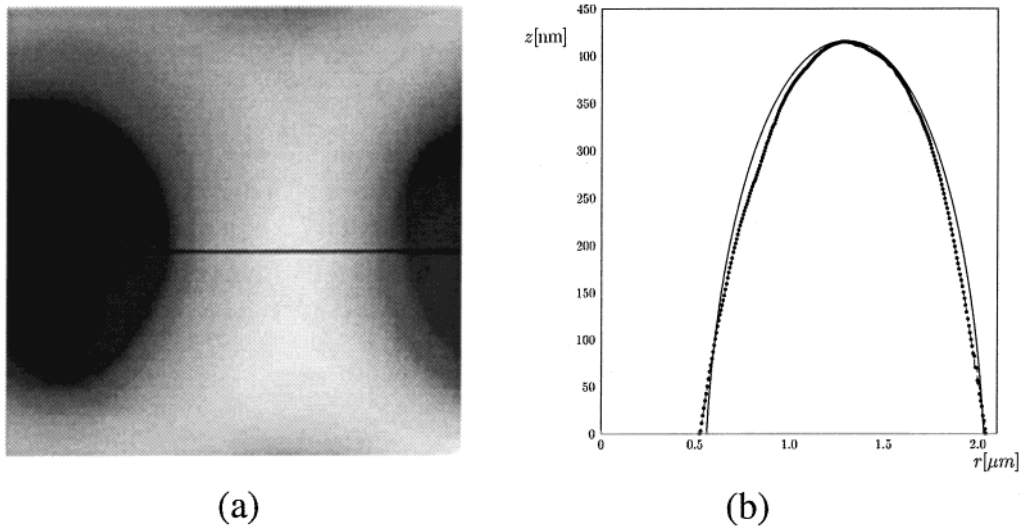**Figure 4.** (a) Enlarged view of a wetting layer as in Figure 3 but with a smaller volume (lateral size of AFM picture, 3 μm $\times$ 3 μm; height, 415 nm). Here, the dark regions represent the nonwetted domains (δ); the light regions are the adsorbate (γ). (b) Corresponding height profile along the straight line in (a) as obtained from the AFM data (symbols) and as calculated within the muffin-tin approximation (solid line); see section 4. The contact angle for this shape is $\theta = 59° \simeq \pi/3$.

In addition, Figure 2b shows the result of the numerical minimization of the free energy (eq 1). The details of the numerical procedure are explained in section 5. The similarities between experiment (Figure 2a) and theory (Figure 2b) are obvious.

A magnified view of the wetting layer as obtained from procedure ii is shown in Figure 4a which displays the shape of the adsorbate (light regions) between two circular lyophobic domains (dark regions). From the cross section along the straight line, we obtained the experimentally determined profile of the wetting layer corresponding to the dark symbols in Figure 4b. It is difficult to estimate the uncertainties of these experimental data: first, the AFM technique has some limited resolution; in addition, the gelation procedure may induce small shape deformations of the wetting layer surface. In any case, we find that these experimental data are in fair agreement with an appropriately chosen segment of a nodoid (Figure 4b, solid line) which is the predicted theoretical solution of the corresponding Laplace equation. This will be shown in the next section where we use an analytical approach to investigate the geometrical properties of this liquid−vapor interface.

4. Analytical Approach

The unit cell of the domain lattice considered here is a square with side length a_γ. The wetting layer morphology has this symmetry as well since it corresponds to a solution of the Laplace equation which is defined on the whole system. Thus, to obtain the shape of the complete $\alpha\beta$ interface one has to find solutions of the shape equation which are defined on the unit cell of the lattice. In general, this two-dimensional nonlinear partial differential equation cannot be solved analytically. However, it is possible to approximate the solutions of this two-dimensional problem by slightly modified solutions of a related one-dimensional problem. This can be achieved by replacing the square unit cell by a circular one. More precisely, the Laplace equation is first solved on an (axisymmetric) circular domain. This solution is then extended to the square unit cell. This procedure resembles the use of the muffin-tin potential for the conduction electrons in a metal. As will be shown below, this approximation turns out to be very good.

4.1. A Model System. To derive this approximate description of the wetting layer configuration, we first consider a model system. It is given by a structured substrate with a single lyophobic domain. To be more precise, the system consists of a circular lyophilic substrate γ with contact angle $\theta_\gamma = 0$. Since this model system will be set in relation to the square unit cell of the lattice, a_γ will be used in this section to denote the diameter of γ, whereas in the next section a_γ will be used to denote the side length of the (quadratic) unit cell of the lattice. Furthermore, γ contains a single circular lyophobic domain δ whose center coincides with the center of γ. The domain has diameter $a_\delta < a_\gamma$, and its contact angle is $\theta_\delta = \pi$. Thus, in this system all wetting layer configurations which dewet δ belong to the droplet regime II. Along the domain boundary of γ, perpendicular walls ϵ with contact angle $\theta_\epsilon = \pi/2$ are added. The whole system is thus a cylinder with a (structured) face at the bottom. In this system, the axisymmetric shape of the wetting layer configuration which dewets δ can be calculated exactly. Determining the $\alpha\beta$ interface is equivalent to finding a surface of constant mean curvature whose boundary is given by two concentric circles with diameters a_δ and a_γ. In three spatial dimensions, any surface which has both constant mean curvature and axial symmetry must be one of the Delaunay surfaces (cf. Appendix), that is, must be a plane, sphere, cylinder, catenoid, unduloid, or nodoid. For the system considered here, the solution must be given by an appropriately chosen segment of a nodoid since the remaining surfaces cannot fulfill the present boundary conditions; compare Figure 5. Nodoid segments also determine the shape of homogeneous channels on lyophilic ring domains as studied in ref 3. The two geometries differ in the boundary conditions at the outer boundary of the γ domain but lead to the same shapes in the limit of large a_γ.

To derive the parametrization of the shape of the wetting layer explicitly, we first choose a parametrization for the nodoids. Then, we discuss the conditions which determine the nodoid segment representing the wetting layer which dewets δ.

If the z axis is parallel to the surface normal of the substrate and if its origin coincides with the center of γ, then the surface of the nodoid is parametrized by the surface vector given by eq A.1. Note that a nodoid is a surface of revolution and therefore its surface is obtained by rotating the curve $z = z_N(r|r_0, r_1)$ around the z axis. The explicit form of z_N is given by eq A.9 of the Appendix, where further details about the parametrization can be found. This curve has two free parameters $r_0 < 0$ and r_1

> 0, where $|r_0|$ is the minimal and r_1 the maximal distance of the curve from the axis of rotation. Thus, $r \in [|r_0|, r_1]$ holds in eq A.9. By periodic continuation of $z_N(r|r_0, r_1)$, one obtains a surface which is defined for all values of z. Surface area A_N and volume V_N of the nodoid are then given by eqs A.10 and A.11. An example of such a nodoid contour is displayed in Figure 5a. In this figure, one segment corresponds to the analytical expression eq A.9, and its periodic continuation leads to the full contour of the axi-symmetric shape (which is, in general, self-intersecting).

Now, the appropriate nodoid segment has to be chosen which represents the $\alpha\beta$ interface of the wetting layer configuration which dewets δ. Geometrically, it can be obtained by cutting the nodoid perpendicular to the z axis locally at $r = |r_0|$; see Figure 5. Mathematically, this corresponds to choosing the values of r_0 and r_1 in such a way that the boundary conditions at the $\gamma\delta$ domain boundary and at the wall ϵ are fulfilled. Since $\theta_\epsilon = \pi/2$, the tangent of the wetting layer has to vanish at the wall ϵ which implies

$$\frac{\mathrm{d}z_N(r|r_0, r_1)}{\mathrm{d}r}\bigg|_{r=a_\gamma/2} = -\frac{r^2 + r_0 r_1}{\sqrt{(r_1^2 - r^2)(r^2 - r_0^2)}}\bigg|_{r=a_\gamma/2} = 0 \tag{2}$$

This condition determines $r_0 = r_0(r_1) = -(a_\gamma/2)^2/r_1$. In addition, one must impose the volume constraint $V = V_N(r|r_0, r_1)$. This can be achieved by adjusting the remaining parameter r_1.

To proceed, denote by θ the contact angle at $r = a_\delta/2$ as defined in Figure 5b,c. Then, the value of θ depends on the choice of the nodoid segment. If the cut is performed at $z > 0$ in Figure 5, one obtains $\theta \leq \pi/2$; for $z < 0$, one obtains $\theta > \pi/2$.

By distinguishing the last two cases, one can derive the remaining formulas which characterize the wetting layer morphology. In eq A.9, the origin is chosen in such a way that $z_N(r = |r_0||r_0, r_1) = 0$ holds. By still restricting the discussion to the droplet regime II, one obtains

$$z^<(r|r_0, r_1) = z_N(r|r_0, r_1) - z_N(r = a_\delta/2|r_0, r_1) \tag{3}$$

for $r \in [a_\delta/2, a_\gamma/2]$ and $\theta_i < \pi/2$.

Surface area and volume of the wetting layer are then given by

$$A_{\alpha\beta}^<(r = a_\gamma/2|r_0, r_1) = A_N(r = a_\gamma/2|r_0, r_1) - A_N(r = a_\delta/2|r_0, r_1) \tag{4}$$

$$V_d^<(r = a_\gamma/2|r_0, r_1) = \pi r^2 z^<(r = a_\gamma/2|r_0, r_1) - V_N(r = a_\gamma/2|r_0, r_1) + V_N(r = a_\delta/2|r_0, r_1) \tag{5}$$

with $r_0 = -(a_\gamma/2)^2/r_1$ in all equations. Furthermore, $A_N(r = |r_0||r_0, r_1) = 0$ and $V_N(r = |r_0||r_0, r_1) = 0$; see Appendix. Similar expressions can be derived for $r < a_\gamma/2$.

The case $\theta > \pi/2$ is slightly more complicated since overhangs have to be taken into account; see Figure 5. The profile must therefore be divided into functions $z_-^>(r|r_0, r_1)$ and $z_+^>(r|r_0, r_1)$. For $r \in [|r_0|, a_\delta/2]$, the β phase lies then between $z_-^>(r|r_0, r_1)$ and $z_+^>(r|r_0, r_1) > z_-^>(r|r_0, r_1)$. Consequently,

$$z_+^>(r|r_0, r_1) = z_N(r|r_0, r_1) + z_N(r = a_\delta/2|r_0, r_1) \tag{6}$$

$$z_-^>(r|r_0, r_1) = z_N(r = a_\delta/2|r_0, r_1) - z_N(r|r_0, r_1) \tag{7}$$
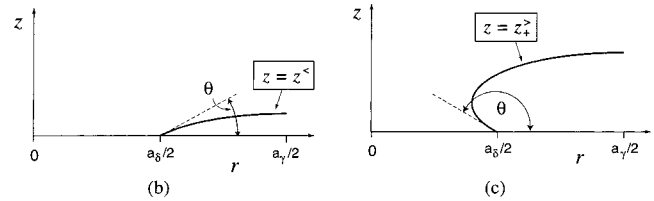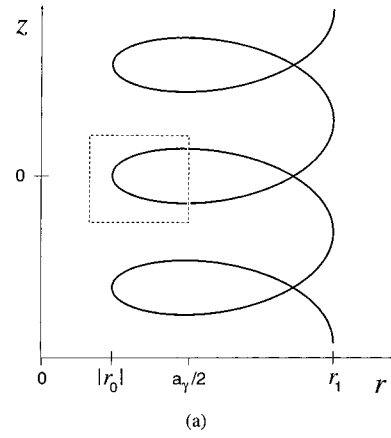

Figure 5. (a) Contour of a nodoid in the (r, z) plane (full line). The complete shape is obtained by rotating this contour around the z axis. The values of the radial r coordinate are restricted to the interval $|r_0| < r < r_1$, and the shape is periodic in the z direction. For the muffin-tin approximation considered here, the only relevant part of the contour corresponds to the "nose" inside the dotted rectangle with $|r_0| < r < a_\delta/2$. (b, c) Two contours of wetting layers close to the lyophobic δ domain with $0 < r < a_\delta/2$. Both contours are obtained by intersection of the nose in (a) with a straight line given by $z = z_{in}$. For $z_{in} > 0$, one obtains a contour as in (b) with contact angle $\theta < \pi/2$. For $z_{in} < 0$, the contour has the shape as shown in (c) with $\theta > \pi/2$.

Surface area and volume are in this case given by

$$A_{\alpha\beta}^>(r = a_\gamma/2|r_0, r_1) = A_N(r = a_\gamma/2|r_0, r_1) + A_N(r = a_\delta/2|r_0, r_1) \tag{8}$$

$$V_d^>(r = a_\gamma/2|r_0, r_1) = \pi r^2 z_+^>(r = a_\gamma/2|r_0, r_1) - V_N(r = a_\gamma/2|r_0, r_1) - V_N(r = a_\delta/2|r_0, r_1) \tag{9}$$

The formulas can be generalized to $r < a_\gamma/2$ where again one has to distinguish between the two profiles. However, one should note that the parameter r_1 which is determined by the volume constraint has to fulfill the inequality $r_1 \geq a_\gamma^2/2a_\delta$, since $|r_0| \leq r \leq r_1$ has to hold. (Our analysis can be extended to the droplet regimes I and III by choosing appropriate boundary conditions. In both regimes, the contact line is detached from the domain boundaries: in regime I, it lies on γ and the contact angle $\theta = \theta_\gamma$; in regime III, it lies on δ with $\theta = \theta_\delta$.)

With this exact solution, the free energy of the $\alpha\beta$ interface can be calculated as a function of the height difference δz between the boundary circles; see Figure 6. One then finds that the configuration of the wetting layer which dewets the lyophobic regions δ exists only up to a critical distance δz_{cr}. Since the volume V is monotonic in δz, this implies that the solution exists only up to a critical volume V^{cr} and corresponding critical contact angle θ^{cr}. Thus, for $V < V^{cr}$ (respectively for $\theta > \theta^{cr}$) the boundary conditions of the dewetted state cannot be fulfilled. Furthermore, for every volume $V < V^{cr}$ two solutions exist; see Figure 6. This behavior originates from the functional
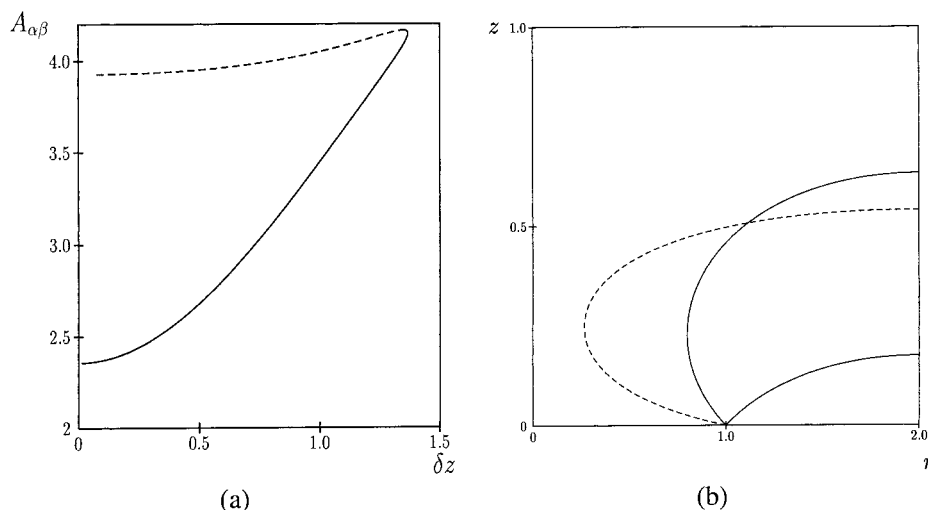
(a)　　　　　　　　　　　　　　　　　　　　　　(b)

Figure 6. (a) Surface area $A_{\alpha\beta}$ of the nodoid segments as a function of the height difference δz of the boundary circles. The solid curve corresponds to the stable branch, the dashed curve to the unstable one. (b) Height profile z as a function of the radial coordinate r for three nodoid segments where the dashed profile corresponds to an unstable configuration. The length scales r, z, and δz are measured in units of the diameter a_δ of the lyophobic δ domain; the area $A_{\alpha\beta}$ is measured in units of a_δ^2. The numerical values displayed in this figure are for $a_\gamma/a_\delta = 2$; in this case, the critical height difference δz_{cr} up to which the dewetted state exists is $\delta z_{cr} \simeq 1.33$.

dependence of $z_+^>(a_\gamma/2)$ on r_1 or $\theta(r_1)$. The function $z_+^>$ is not monotonic in θ but exhibits a maximum.

This behavior of the solution is characteristic for systems where the boundary conditions correspond to geometrical constraints. In the case studied here, one wants to obtain a surface which is bounded by two circles and exhibits a certain contact angle at the larger circle. This is very similar to the well-known problem of finding a minimal surface (i.e., a surface of zero mean curvature) which is bounded by two coaxal circles of identical diameter. In the latter case, one obtains a catenoid for sufficiently small distances of the circles. To be more precise, one obtains two catenoids, a stable and an unstable one.[23] In fact, these two solutions are also found if the boundaries of the minimal surface are given by two coaxal circles with different diameters provided their height difference $z_+^>(a_\gamma/2)$ is sufficiently small.

4.2. Extension to the Lattice. To obtain an approximate description of the wetting layer morphology on the complete array of lyophobic domains, one has to extend this special solution (of the circular unit cell) to the square unit cell with length a_γ. Since the square unit cell is not axisymmetric, this extension breaks the rotational symmetry. However, if one assumes that for $r \leq a_\gamma/2$ the breaking of the axial symmetry is only weak, then the above solution can be used as an ansatz for $r \leq a_\gamma/2$. On the remaining part of the unit cell, a plane can then be used as extension. In this case, the solution stays differentiable since $dz/dr = 0$ holds at $r = a_\gamma/2$. One expects this approximation to become exact for large a_γ, but in fact it also yields good results for small a_γ.

To proceed, introduce local Cartesian coordinates (x, y) with origin $(0, 0)$ at the center of every unit cell. Then, for $|x| \leq a_\gamma/2$ and $|y| \leq a_\gamma/2$ the approximate ("muffin-tin") solution on the lattice is given by

$$z_L(r|r_0, r_1) = z(r|r_0, r_1)H(a_\gamma/2 - r) +$$
$$z(r = a_\gamma/2|r_0, r_1)\, H(r - a_\gamma/2) \quad (10)$$

where $r \equiv \sqrt{x^2 + y^2}$ and $H(x)$ denotes the Heaviside function, that is, $H(x) = 1$ for $x > 0$, $H(x) = 0$ for $x < 0$,

and $H(0) = 1/2$. Here, again one has to distinguish between $\theta \leq \pi/2$ and $\theta > \pi/2$ and between $r \leq a_\delta/2$ and $r > a_\delta/2$. Correspondingly, $z = z^<$ or $z = z_\pm^>$ holds in the last equation depending on the values of θ and r. The surface area A_L and the volume V_L per unit cell can be derived similarly for the different cases. Equation 10 holds only for quadratic unit cells, but it is straightforward to generalize the analysis to triangular lattices or even more general lattice structures.

By restricting the solution to be constant for $r > a_\gamma/2$, one makes an error, since one does not take into account the mean curvature of the $\alpha\beta$ interface along the side boundaries of the unit cell, that is, between the points $(x, y) = (a_\gamma/2, 0)$ and $(x, y) = (a_\gamma/2, a_\gamma/2)$. However, $|r_0| \leq a_\delta/2$ and $r_1 \geq a_\gamma/2$ and eq A.8 implies

$$M \leq \frac{2/a_\delta}{a_\gamma/a_\delta - 1} \quad (11)$$

Hence, in the limit of large a_γ/a_δ at constant a_δ this error becomes small.

5. Numerical Investigation and Discussion

To show that this analytical approximation captures the essential properties of the wetting layer morphology, we also calculated the shape of the $\alpha\beta$ interface by direct numerical minimization of the free energy functional (eq 1). In principle, one should be able to do this using available software packages such as the Surface Evolver.[24] In practice, we found it more convenient to use a slight modification of the numerical algorithm which we developed previously for a different domain geometry.[2] Using the latter code, we determined the wetting layer morphology of minimal surface area which (i) fulfills the boundary conditions arising from the structured substrate and which (ii) has a given volume V.

One example for the wetting layer morphology found by this method is presented in Figure 7a, which demonstrates that the Laplace equation indeed has solutions of high topological genus.

(23) Taylor, G. I.; Michael, D. H. *J. Fluid Mech.* **1973**, *58*, 625.

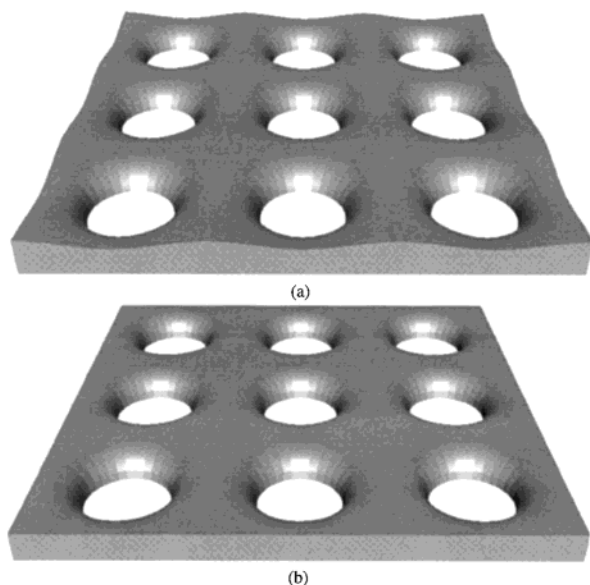(24) Brakke, K. *Exp. Math.* **1990**, *1*, 141.

Figure 7. The wetting layer morphology which dewets the lyophobic regions (δ) as determined numerically (a) and as given by the analytical approximation (b). In both cases, the parameters are chosen to be $a_\gamma/a_\delta = 2$, $V/(a_\delta^3) = 1$, $\theta_\gamma = 0$, and $\theta_\delta = \pi$.

On the other hand, Figure 7b shows the wetting layer morphology corresponding to the approximate muffin-tin solution. Direct inspection of Figure 7 shows that the two solutions look quite similar and that the approximate solution captures the main features of the numerical solution. In addition to the obvious similarity between parts a and b of Figure 7, the surface area of the dewetted states as a function of the adsorbate volume is identical for both solutions; see Figure 8a,b. This underlines the excellent agreement of the two approaches.

The numerical lattice solution has the same properties as the solution of the single-domain system. In particular, the dewetted state exists only for a certain volume range $V < V^{tr}$; see Figure 8. This is in agreement with the experimental and the analytical investigation.

Furthermore, the numerically, analytically, and experimentally obtained morphologies show the same characteristics, as is evident from Figures 2a,b, 3, and 7a,b. A closer inspection of for example Figures 2a,b and 3 reveals that both the numerically and the experimentally obtained morphologies show slightly elevated regions between the lyophobic domains. The analytical approximation neglects these regions, as displayed in Figure 7a,b. However, eq 11 implies and the excellent agreement between the approximate and the numerical solution shows that the contributions to the physical quantities arising from these regions are negligible. Furthermore, the geometrical characteristics of the wetting layer do not seem to have a strong dependence on the details of the lattice structure; see Figure 2a and Figure 3. This is supported by the finding that the experimentally measured height profile on a triangular lattice is in excellent agreement with the height profile obtained within the muffin-tin approximation; cf. Figure 4.

The analysis presented here can be extended to study morphological wetting and dewetting transitions in these systems. In this case, one has to take competing states into account: the perforated film state, the completely covering film, and patterns of droplets. These droplets have the shape of spherical caps, and their contact areas are completely contained within the γ domains. For $\theta_\gamma = 0$, only the first two states fulfill the boundary conditions.

The energy of the completely covering film state is equal to that of the unstable branch of the dewetted state with vanishing volume V; see also Figure 8. This is a consequence from the fact that for small V, the $\alpha\beta$ interface of the unstable branch attains a limit shape which consists of a thin layer with small pores above the lyophobic surface domains. As V goes to zero, the $\alpha\beta$ interface touches the lyophilic γ domains (i.e., $\vec{z}_+(r = a_\gamma/2|r_0, r_1)$ vanishes) and folds onto itself above the lyophobic δ domains. At the same time, the pores close (since r_0 vanishes as V goes to zero) and the surface area of the $\alpha\beta$ interface becomes equal to the area of the γ domains plus twice the area of the δ domains. Thus, the perforated film has a free energy $F_p/\Sigma_{\alpha\beta} = A_L(V) - A_{\beta\delta}\cos\theta_\delta$ with $A_{\beta\delta} = a_\gamma^2 - \pi(a_\delta/2)^2$ whereas the film state has a free energy $F_{fi}/\Sigma_{\alpha\beta} = A_L(V = 0) - A_{\beta\delta}\cos\theta_\delta$. Thus, the transition between these two states takes place at a volume $V_c < V^{tr}$ (which corresponds to a critical film height l_c) with $A_L(V = 0) = A_L(V = V_c)$. The transition is first order and shows hysteresis effects.

For $\theta_\gamma > 0$, spherical caps on γ are an additional alternative to the connected dewetted state. Our experimental investigation shows that this state dominates for small volumes V.

For large ratios a_γ/a_δ and sufficiently large contact angles θ_γ, the droplet state will make a direct transition to the completely wetting film state. Therefore, the film state which dewets the δ regions will not be experimentally observable. Finally, for smaller ratios a_γ/a_δ, for example, larger lyophobic areas, and appropriately chosen small values of θ_δ with $\pi/2 < \theta_\delta < \pi$, droplet regime III (in which $\theta = \theta_\delta$) does not exist since then the completely covering film state is energetically favored.

In the present geometry, the mean curvature of the wetting layer seems to have, as a function of the contact angle θ, only one stable branch which is terminated by other, competing states. If the breaking of axial symmetry is only small for $r \le a_\gamma/2$, as assumed above, then there is no analytical evidence that the wetting layer morphology can become unstable with respect to the development of bulges in contrast to the case of liquid channels; see refs 2 and 3. The experimental and numerical investigation support this conjecture.

6. Summary and Outlook

In summary, we have investigated the geometric properties of wetting layer morphologies on substrates consisting of lyophobic patches in a lyophilic matrix. For sufficiently small liquid volumes, a perforated film with many holes is present which is investigated both experimentally and theoretically.

By using a sol−gel technique, we deposited wetting liquids, which undergo a subsequent solidification process upon exposure to air humidity, on chemically patterned substrates. Afterwards, the topography of the samples was investigated by atomic force microscopy.

In addition, we have performed a detailed mathematical analysis of the geometrical shape of the wetting layer. We demonstrate that the Laplace equation has solutions of high topological genus, that is, solutions with many holes. The results of the approximate analytical calculations are in excellent agreement both with those of numerical calculations and with the experimental data.

By comparing this system with those studied earlier, one sees that the topology of the substrate influences its phase diagram. Since the dewetted or perforated film state is topologically connected, it has to fulfill rather different boundary conditions. These conditions restrict the volume range in which the perforated film state exists. Thus, the dominating state of the system is the film with uniform
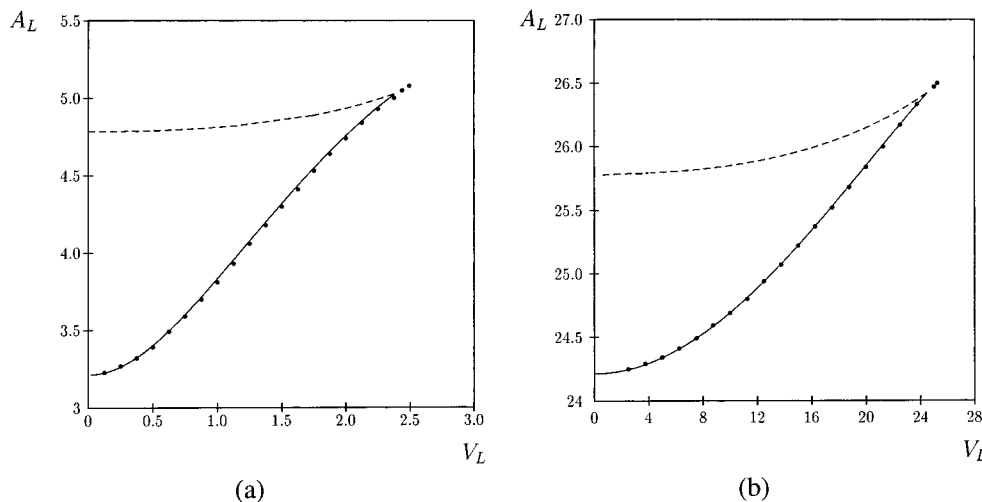
Figure 8. The surface area A_L (per unit cell) of the $\alpha\beta$ interface of the dewetted state as function of its volume V_L (per unit cell). The solid curve corresponds to the analytical muffin-tin solution; the points correspond to the results of the numerical minimization. The data in (a) and (b) are for $a_\gamma/a_\delta = 2$ and $a_\gamma/a_\delta = 5$, respectively. In both cases, the dashed line represents the branch of the unstable solution. Here, A_L is measured in units of a_δ^2, V in units of a_δ^3.

thickness since it exists for all volumes V and has minimal energy for $V > V^{cr}$.

Finally, the classification of constant mean curvature surfaces with complex topologies is a timely subject in differential geometry (see, for example, refs 25−27), and similar surfaces also play a role in other physical systems such as, for example, two-component membranes.[28] The results derived here might also be useful for the investigation of the breakup of films, as studied in refs 10 and 29. Indeed, our calculations show that axisymmetric holes disturb the whole film. This is a consequence of the fact that there is no axisymmetric liquid−vapor interface with holes which has vanishing mean curvature $M = 0$; compare section 4. Since a flat film fulfills $M = 0$, a hole cannot be axisymmetric if it disturbs the film only locally.

Appendix: The Surfaces of Delaunay

The French mathematician Delaunay was the first to prove that there are exactly six different two-dimensional surfaces of revolution which have constant mean curvature.[30] These are planes, catenoids (both with vanishing mean curvature), spheres, cylinders, unduloids, and nodoids (all with nonvanishing mean curvature). This fact is often mentioned in textbooks on differential geometry, but explicit parametrizations for unduloids and nodoids are difficult to find. In this appendix, we will describe such a parametrization which is equivalent to the one used in ref 31.

A two-dimensional surface of revolution can be parametrized by a surface vector

$$R(z, \varphi) = (r(z) \cos \varphi, r(z) \sin \varphi, z) \quad (A.1)$$

Then, the mean curvature is given by[32]

$$M = -\frac{rr_{zz} - (1 + r_z^2)}{2r(1 + r_z^2)^{3/2}} \quad (A.2)$$

where the sign is chosen in such a way that a sphere of radius R has positive mean curvature $M = 1/R$. Here, $r_z \equiv dr/dz$, $r_{zz} \equiv d^2r/dz^2$. By introducing the inverse function $z = z(r)$ and by using the substitution $y = 1 + 1/z'^2$, $z' \equiv dz/dr$, one can transform the last equation to a differential equation of Bernoulli type in y. Then, by solving it one obtains the first integral of eq A.2.

$$\frac{dz}{dr} = \frac{Mr^2 + C_1}{\sqrt{r^2 - (Mr^2 + C_1)^2}} \equiv \frac{r^2 + b^2}{\sqrt{4a^2r^2 - (r^2 + b^2)^2}} \quad (A.3)$$

where C_1 is a constant of integration. The solutions of this differential equation correspond to the sought surfaces. The last equation can be interpreted geometrically.[33] If an ellipse is rolled along a line, its focus describes a curve $z(r)$ given by the last equation. The semimajor axis a and b (with $a > b$) of the ellipse determines the constant C_1; cf. the right-hand side of eq A.3. By introduction of the maximum $r_1 \equiv a + \sqrt{a^2 - b^2}$ and minimum distance $r_0 \equiv a - \sqrt{a^2 - b^2}$ of the focus from the axis of rotation, eq A.3 can be integrated.[34] Then, for $r \in [r_0, r_1]$, the solution corresponds to an unduloid as given by

$$z_U(r|r_0, r_1) = r_0 F(\kappa, p) + r_1 E(\kappa, p) - \frac{1}{r}\sqrt{(r_1^2 - r^2)(r^2 - r_0^2)} \quad (A.4)$$

$$A_U(r|r_0, r_1) = 2\pi(r_0 + r_1)\left(r_1 E(\kappa, p) - \frac{1}{r}\sqrt{(r_1^2 - r^2)(r^2 - r_0^2)}\right) \quad (A.5)$$

(25) Grosse-Brauckmann, K.; Polthier, K. *Exp. Math.* **1997**, *6*, 13.
(26) Grosse-Brauckmann, K.; Kusner, R. B.; Sullivan, J. M. *Proc. Natl. Acad. Sci. U.S.A.* **2000**, *97*, 14067.
(27) Kilian, M.; McIntosh, I.; Schmitt, N. *Exp. Math.* **2000**, *9*, 595.
(28) Góźdź, W. T.; Gompper, G. *Phys. Rev. Lett.* **1998**, *80*, 4213.
(29) Jacobs, K.; Seeman, R.; Schatz, G.; Herminghaus, S. *Langmuir* **1998**, *14*, 4961.
(30) Delaunay, C. *J. Math. Pures Appl. Sér.* **1841**, *1*, 309.
(31) Roe, R.-J. *J. Colloid Interface Sci.* **1975**, *50*, 70.

(32) Dierkes, U.; Hildebrandt, S.; Küster, A.; Wohlrab, O. *Minimal Surfaces I*; Springer-Verlag: Berlin, 1992.
(33) Loria, G. *Curve piane speciali*; U. Hoepli: Milano, 1930.
(34) Gradshteyn, I. S.; Rhyzik, I. M. *Table of integrals, series and products*, 5th ed.; Academic Press: San Diego, CA, 1994.

$$V_U(r|r_0, r_1) = \frac{\pi}{3}\Big\{E(\kappa, p)(3r_0r_1^2 + 2r_1^3 + 2r_1r_0^2) -$$

$$r_1r_0^2 F(\kappa, p) - \frac{1}{r}\sqrt{(r_1^2 - r^2)(r^2 - r_0^2)}(3r_0r_1 + r^2 +$$

$$2r_1^2 + 2r_0^2)\Big\} \quad (A.6)$$

(The results derived here are equivalent to those obtained in ref 31.) Here,

$$\kappa \equiv \arcsin\sqrt{\frac{r_1^2(r^2 - r_0^2)}{r^2(r_1^2 - r_0^2)}} \qquad p \equiv \frac{\sqrt{r_1^2 - r_0^2}}{r_1} \quad (A.7)$$

and F and E denote elliptic integrals of the first and second kind, respectively:[34]

$$F(\kappa, p) = \int_0^\kappa \frac{d\alpha}{\sqrt{1 - p^2\sin^2\alpha}} =$$

$$\int_0^{\sin\kappa} \frac{du}{\sqrt{(1 - u^2)(1 - p^2u^2)}}$$

$$E(\kappa, p) = \int_0^\kappa d\alpha\sqrt{1 - p^2\sin^2\alpha} = \int_0^{\sin\kappa} du\sqrt{\frac{1 - p^2u^2}{1 - u^2}}$$

As can be easily checked, the mean curvature then fulfills

$$M = \frac{1}{r_1 + r_0} \quad (A.8)$$

A nodoid is obtained by rolling a hyperbola, which can be seen as an ellipse with complex main axis $b = i|b|$. Here, the curve described by the focus is given by

$$dz = -\frac{r^2 + r_0r_1}{\sqrt{(r_1^2 - r^2)(r^2 - r_0^2)}}\,dr$$

with $r_0 < 0$ and $r \in [|r_0|, r_1]$. By using the notation introduced above, one obtains

$$z_N(r|r_0, r_1) = -r_0 F(\kappa, p)\, r_1 E(\kappa, p) +$$

$$\frac{1}{r}\sqrt{(r_1^2 - r^2)(r^2 - r_0^2)} \quad (A.9)$$

$$A_N(r|r_0, r_1) = 2\pi(r_0 + r_1)\Big(r_1 E(\kappa, p) -$$

$$\frac{1}{r}\sqrt{(r_1^2 - r^2)(r^2 - r_0^2)}\Big) \quad (A.10)$$

$$V_N(r|r_0, r_1) = -\frac{\pi}{3}\Big\{E(\kappa, p)(3r_0r_1^2 + 2r_1^3 + 2r_1r_0^2) -$$

$$r_1r_0^2 F(\kappa, p) - \frac{1}{r}\sqrt{(r_1^2 - r^2)(r^2 - r_0^2)}(3r_0r_1 + r^2 +$$

$$2r_1^2 + 2r_0^2)\Big\} \quad (A.11)$$

In both cases, a surface defined for arbitrary z can be obtained by periodic continuation. Finally, one should note that cylinder and sphere are special cases of the unduloid, which are obtained for $(r_0 = r_1)$ and $(r_0 = 0)$, respectively. The nodoid becomes a catenoid in the limit of large r_1.

List of Mathematical Symbols

a_δ	diameter of lyophobic δ domain
a_γ	diameter of lyophilic γ domain in the muffin-tin approximation corresponding to lattice constant of surface domain lattice
α	fluid bulk phase
A	interfacial area
A_L	area of $\alpha\beta$ interface per unit cell of lattice
β	wetting liquid phase
δ	lyophobic surface domain with contact angle θ_δ
δz	height difference of boundary circles
δz_{cr}	largest possible height for perforated wetting layer
ϵ	confining walls with contact angle θ_ϵ
γ	lyophilic surface domain with contact angle θ_γ
H	Heaviside step function
κ	parameter for unduloid and nodoid as used in Appendix
M	mean curvature
p	parameter for unduloid and nodoid as used in Appendix
r	radial coordinate for axially symmetric shapes in muffin-tin approximation
r_0, r_1	parameters for the nodoid shape, see Figure 5
Σ	interfacial tension
θ	contact angle
θ^{cr}	largest possible contact angle for perforated wetting layer
θ_δ	contact angle on the lyophobic δ domains with $\theta_\delta > \pi/2$
θ_γ	contact angle on the lyophilic γ domains with $\theta_\gamma < \pi/2$
V	volume of wetting liquid
V^{cr}	largest possible volume for perforated wetting layer
V_L	volume per unit cell of lattice
z	height of wetting layer
$z_N(r|r_0, r_1)$	parametrization of nodoid with free parameters r_0 and r_1
$z^<$	height profile of wetting layer for $\theta < \pi/2$
$z_+^>, z_-^>$	two height profiles describing wetting layer shapes with overhangs for $\theta > \pi/2$